Evaluation of Bogus Vortex Techniques with Four-dimensional Variational Data Assimilation

Zhao-Xia Pu*

Universities Space Research Association

Mesoscale Atmospheric Processes Branch

Laboratory for Atmospheres

NASA Goddard Space Flight Center

Scott A. Braun

Laboratory for Atmospheres

NASA Goddard Space Flight Center

Submitted to

Monthly Weather Review

February 12, 2000

---

* *Corresponding Author:* Dr. Zhao-Xia Pu, NASA/GSFC, Code 912, Greenbelt, MD 20771.

E-mail: pu@gilbert.gsfc.nasa.gov

ABSTRACT

The effectiveness of techniques for creating "bogus" vortices in numerical simulations of hurricanes is examined by using the Penn State/NCAR nonhydrostatic mesoscale model (MM5) and its adjoint system. A series of four-dimensional variational data assimilation (4-D VAR) experiments is conducted to generate an initial vortex for Hurricane Georges (1998) in the Atlantic Ocean by assimilating bogus sea-level pressure and surface wind information into the mesoscale numerical model. Several different strategies are tested for improving the vortex representation.

The initial vortices produced by the 4-D VAR technique are able to reproduce many of the structural features of mature hurricanes. The vortices also result in significant improvements to the hurricane forecasts in terms of both intensity and track. In particular, with assimilation of only bogus sea-level pressure information, the response in the wind field is contained largely within the divergent component, with strong convergence leading to strong upward motion near the center. Although the intensity of the initial vortex seems to be well represented, a dramatic spin down of the storm occurs within the first 6 h of the forecast. With assimilation of bogus surface wind data only, an expected dominance of the rotational component of the wind field is generated, but the minimum pressure is adjusted inadequately compared to the actual hurricane minimum pressure. Only when both the bogus surface pressure and wind information are assimilated together does the model produce a vortex that represents the actual intensity of the hurricane and results in significant improvements to forecasts of both hurricane intensity and track.

When the scale of the specified bogus vortex is smaller than that which can be resolved

by the model, the assimilation method may result in structures that do not completely resemble observed structures in hurricanes. An example is the vertical motion field, which for a smaller-scale vortex, tends to be characterized by upward motion at the center of the hurricane. An additional numerical experiment indicates that a relatively larger vortex size assignment that allows for improved resolution of the vortex on a mesoscale grid leads to a more realistic depiction of the vertical motion field and to significant improvement of the hurricane track forecast.

Finally, the bogusing methodology is further evaluated by applying it to Hurricane Bonnie (1998) just prior to its rapid intensification. The bogus vortex improves the track and intensity forecasts for Bonnie, but is not quite able to capture the correct rate of deepening. These results stress the need to incorporate additional information from satellites and aircraft.

1. Introduction

Forecasts of track and intensity changes for mature hurricanes require accurate representation of the hurricane vortex in model initial conditions. Vortices contained in large-scale analyses from operational centers are often too weak and sometimes misplaced and observations in the vicinity of the hurricane are usually sparse. In order to improve the storm representation, the use of so-called "bogus vortices" is often adopted (Lord 1991; Kurihara et al. 1990; Leslie and Holland 1995). A bogus vortex is an artificial vortex generated by knowledge of an empirically realistic vortex. It is usually specified based on the size of the cyclone (the radius of maximum winds), its position, and its intensity (the maximum velocity or minimum sea-level pressure). Traditionally, such bogus vortices have been directly implanted into the larger-scale environment. Many successful simulations, including prediction of hurricane movement and structure, have been conducted using bogus vortices for hurricane model initialization (e.g., Kurihara et al. 1990; Lord 1991; Trinh and Krishnamuti 1992). However, an important and unsolved issue in such an approach is consistency of the vortex with the properties of the prediction model. The initial moisture field, which can affect the intensity change of the vortex, has been especially difficult to specify in a realistic yet model-consistent manner (Iwasaki et al. 1987; Mathur 1991).

A more advanced scheme has been proposed by Kurihara et al. (1993) at the Geophysical Fluid Dynamics Laboratory (GFDL) to overcome such defects. The main strategy of their scheme is to replace the poorly resolved vortex from a coarse-resolution analysis with a more realistic vortex that is constructed to match better the high-resolution hurricane prediction model.

They apply two spatial filters to remove the poorly resolved vortex from the large-scale analysis. The specified vortex to be placed in the environmental field consists of a symmetric vortex and an asymmetric flow. The symmetric component is generated from a time integration of an axisymmetric version of the hurricane prediction model, with an observationally derived constraint imposed on the tangential flow. The generated symmetric wind is used in the computation of the asymmetric component using a simplified barotropic vorticity equation, thus providing consistent symmetric and asymmetric components. The mass field is then recomputed using a static initialization method in which the generated wind field is not modified. This technique, proposed by Kurihara et al. (1993), ensures the following desirable conditions: 1) a smooth transition between the environmental field and the storm area; 2) compatibility of the specified vortex to the resolution and physics of the prediction model; 3) structural consistency of the generated vortex in the fields of wind, temperature, surface pressure, and moisture; and 4) the incorporation of realistic features in the tangential flow of the vortex. As anticipated, the method shows a substantial improvement in the track prediction (Bender et al. 1993). The success of this technique indicates the importance of having a dynamically and thermodynamically consistent initial vortex that is compatible with the resolution and physics of the hurricane prediction model.

As a natural extension of the GFDL's initialization method, Zou and Xiao (2000) have proposed a new approach to improve the initial vortex by using a four-dimensional variational data assimilation technique (4-D VAR). The method requires two steps: 1) Specification of a bogus vortex by defining the position, radius of maximum wind and minimum sea-level pressure of the initial vortex, and prescribing a symmetric sea-level pressure distribution over the vortex

region; 2) assuming that the time tendency of sea-level pressure is near zero in a short time period and then assimilating the specified bogus sea-level pressure field into the numerical model within a 30-minute assimilation window. They show very encouraging results for Hurricane Felix (1995).

The advantages of using the 4-D VAR technique to generate the bogus vortex are as follows. First, the 4-D VAR technique uses the actual forecast model rather than a simplified model (e.g., an axisymmetric model) to provide a strong dynamical constraint during the bogus data assimilation. Observational data, bogus information and model dynamics are combined in one system. The assimilation results not only fit the data but also are consistent with the model resolution and physics. Second, the 4-D VAR technique allows all model variables to be adjusted freely during the assimilation period. Finally, the 30-min assimilation window allows the initially symmetric vortex to develop asymmetric structure.

Since the 4-D VAR method shows promise for vortex initialization, this study explores the effectiveness of the bogusing technique of Zou and Xiao (2000) for the case of Hurricane Georges (1998) and examines the sensitivity of the results to vortex size and the type of bogus information (pressure, wind). Considering the large computational expense required for 4-D VAR data assimilation, the experiments are performed at relatively coarse horizontal grid resolution in this study.

Brief descriptions of the methodology and model are described in section 2, and a summary of Hurricane Georges is given in section 3. Evaluation of model sensitivity to the bogus vortex scheme is given in section 4. The impacts of vortex size on the initialization and forecast are investigated in section 5. To demonstrate the effectiveness of the methodology in the

case of a rapidly deepening storm, the bogusing technique is applied to the case of Hurricane Bonnie (1998) in section 6. A summary is given in section 7.

2. A variational bogus vortex scheme

Following Zou and Xiao (2000), the bogus vortex scheme consists of two steps: 1) Bogus vortex data specification and 2) 4-D VAR assimilation of the bogus data.

a. Vortex Specification

The bogus "observations'' for the specified initial vortex consist of values of sea-level pressure and wind speed and direction over a circular region with a radius R. The vortex is assumed to be axisymmetric. The surface pressure field is specified based upon the radius of maximum wind in the cyclone, the position of the hurricane center, and central pressure. In general, the distribution of bogus sea-level pressure data can be generated by empirical functions such as the formulas of Fujita's or others (Holland 1980; Anthes, 1982). In this study, the hurricane sea-level pressure is specified following the analytic model proposed by Holland (1980).

According to Holland (1980), the sea-level pressure, p^{bogus}, at radius r ($0 \le r \le R$) is defined by the following relationship

$$p^{\text{bogus}}(r) = p_c + (p_n - p_c)\exp(-A/r^B), \tag{1}$$

where p_c the central sea-level pressure and p_n the ambient pressure (theoretically at infinite radius; however, in practice, the value of the first anticyclonically curved isobar is used). The

scaling parameters A and B are defined by maximum wind information as follows. Using the gradient balance relationship and Eq. (1), the wind profile is

$$V_g^{\text{bogus}}(r) = \left[AB(p_n - p_c)\exp(-A/r^B)/\rho r^B + r^2 f^2/4\right]^{1/2} - rf/2, \qquad (2)$$

where V_g^{bogus} is the gradient surface wind at radius r, f is the Coriolis parameter, and ρ the air density (assumed constant at 1.15 g m^{-3}). In the region of maximum winds, the Coriolis force is small in comparison to the pressure gradient and centrifugal forces and the air is in cyclostrophic balance. These winds are given by

$$V_g^{\text{bogus}}(r) = \left[AB(p_n - p_c)\exp(-A/r^B)/\rho r^B\right]^{1/2} \qquad (3)$$

By setting $dV_g/dr = 0$, the radius of maximum winds is $R_m = A^{1/B}$ and substitution back into (3) gives the maximum wind speed, $V_m = C(p_n - p_c)^{1/2}$, where $C = (B/\rho e)^{1/2}$ and e is the base of natural logarithms. Specification of V_m and R_m then provides values of A and B for Eqs. (1-2).

A vertical profile is assumed for the wind information in order to extend the information to higher levels. Following Kurihara et al. (1993), the vertical structure of the wind is specified by an empirical function $F(\sigma)$ as follows:

$$V_g^{\text{bogus}}(r,\sigma) = F(\sigma)V^{\text{bogus}}{}_g(r) \qquad (4)$$

where σ denotes the vertical level. The numerical values of $F(\sigma)$ can be modified according to the storm depth (Kurihara et al. 1993). Further details are given in Section 4.

b. Variational assimilation of the bogus vortex data

The bogus distributions of pressure and wind are introduced into the 4-D VAR assimilation system within a 30 min assimilation window. The cost function to be minimized is written as follows:

$$J = \sum_{k=1,m} J_k + J_b \tag{5}$$

where J_b is the background error covariance term and J_k is the contribution to the cost function from a certain type of data. The subscript k denotes the type of data and m is the total number of available data types. For example, the contribution from bogus sea-level pressure and wind information can be described as follows:

$$J_1 = \sum_{t_\tau} \sum_{i,j \in R} \left(p - p^{\text{bogus}}\right)^T W_p \left(p - p^{\text{bogus}}\right), \tag{6}$$

$$J_2 = \sum_{t_\tau} \sum_{(r,\sigma) \in R} \left(V - V_g^{\text{bogus}}(r,\sigma)\right)^T W_V \left(V - V_g^{\text{bogus}}(r,\sigma)\right), \tag{7}$$

where p and V are the analysis variables, p^{bogus} and V^{bogus} are the bogus vortex data, τ and $\kappa \in (0,\Delta)$ are the observation times, while Δ is the length of assimilation window. W_p and W_V are weighting factors that depend on the assumed statistical error characteristics of the bogus data.

In this study, J_b is a simple background term measuring the distance between the model state and the MM5 analysis based on the large-scale ECMWF analysis. Only approximated variances are included in the background weighting matrix. The weighting factors W_p and W_V are diagonal weighting matrices and their values are determined empirically.

c. The numerical forecast model and its adjoint

The PSU/NCAR mesoscale forecast model (MM5) and its adjoint system are used in this study. The MM5 is a limited-area, non-hydrostatic primitive equation model with multiple options for various physical parameterization schemes (Dudhia 1993; Grell et al. 1995). The model employs a terrain-following σ vertical coordinate, where σ is defined as $\sigma = (p - p_{top})/(p_{sfc} - p_{top})$, p is pressure, and p_{sfc} and p_{top} are the pressures at the surface and model top, respectively. Physics options used for this study include the Betts-Miller cumulus parameterization, a simple ice microphysics scheme (Dudhia 1989), the Blackadar high-resolution planetary-boundary layer parameterization scheme (Blackadar, 1976, 1979; Zhang and Anthes 1982), and the cloud atmospheric radiation scheme (Dudhia 1993). The land surface temperature is predicted using surface energy budget equations as described in Grell et al. (1995). For a more detailed description of MM5, the reader is referred to Dudhia (1993) and Grell et al. (1995).

The MM5 adjoint modeling system (Zou et al. 1998) is employed in the data assimilation experiment. For the variational data assimilation system, physics options are limited to the Kuo cumulus parameterization and a simple bulk-aerodynamic planetary boundary layer scheme. Application of the MM5 adjoint model to a variety of mesoscale weather systems has been demonstrated in papers by Zou et al. (1995), Kuo et al. (1996), and Zou and Xiao (2000).

3. Summary of Hurricane Georges (1998)

Georges was the second deadliest and second strongest hurricane within the Atlantic

basin during the 1998 season. During its 17-day lifetime (15 September – 01 October), it resulted in multiple landfalls, extending from the northeastern Caribbean to the coast of Mississippi, and 602 fatalities, mainly in the Dominican Republic and Haiti.

Because of an interest in examining the landfall of Georges in Puerto Rico and Hispaniola, 1200 UTC 21 September 1998 was selected as the initial time for simulation. At this time, Georges was located over the ocean to the east-southeast of Puerto Rico (Fig. 1) and was a mature category 2 hurricane based on the Saffir-Simpson intensity scale, having recently weakened from a category 4 intensity. Georges eyewall made landfall in Puerto Rico with sustained surface winds in excess of 50 m s^{-1} late on the 21st. The hurricane moved inland over Puerto Rico, weakened slightly, and then moved into the Mona Passage early on the 22nd, where it re-intensified slightly before making landfall later that morning in the Dominican Republic with estimated sustained surface winds of 54 m s^{-1}. During the next 21 h, George weakened as it moved slowly across the mountainous terrain of the Dominican Republic and Haiti, where it produced copious rain, deadly flash floods, and mud slides. The system moved into the Windward Passage on the morning of the 23rd with maximum sustained winds reduced to 33 m s^{-1}. Georges changed little before making landfall in eastern Cuba later that afternoon (Fig. 1).

4. Evaluation of the variational bogus vortex scheme

a. Experimental design

For the experiments, two horizontal grids are used, a fixed outer domain A, with a 36-km grid spacing, and a nested, movable inner mesh B with a 12-km grid spacing (Fig. 1). The model vertical structure is comprised of 27 σ levels with the top of the model set at a pressure of 50

hPa. The σ levels are placed at values of 1.0, 0.99, 0.98, 0.96, 0.93, 0.89, 0.85, 0.81, 0.77, 0.73, 0.69, 0.65, 0.61, 0.57, 0.53, 0.49, 0.45, 0.41, 0.37, 0.33, 0.29, 0.25, 0.21, 0.17, 0.13, 0.09, 0.05, and 0. The assimilation of the bogus vortex information is applied only to the 36-km domain. At the end of the assimilation window (30 min), the 12-km nest is initialized by interpolation (see Grell et al. 1995) of all prognostic variables from the 36-km mesh using a monotonic interpolation scheme based upon Smolarkiewicz and Grell (1992). All figures present results from the 12-km grid.

Initial conditions for the 36-km domain, prior to assimilation, are derived from 12-h European Center for Medium-Range Forecasts (ECMWF) analyses archived at NCAR. Analysis fields, including temperature, relative humidity, geopotential height, and winds at mandatory pressure levels and with horizontal resolution of 2.5°×2.5°, are interpolated horizontally to model grid points. These interpolated analyses are refined by adding information from standard twice daily rawinsondes and 3-hourly surface and buoy reports using a Barnes objective analysis technique (Manning and Haagenson, 1992). Final analyses are then interpolated to the model σ levels. Figure 2a shows the ECMWF analysis fields of sea-level pressure and 850-hPa wind vectors and wind speed at 1200 UTC 21 September 1998. At the time, Hurricane George was a category 2 hurricane, but the ECMWF analysis shows only a weak pressure minimum (about 1008 hPa) and a broad wind speed maximum to the northeast of the center.

Several experiments are conducted using the variational bogus vortex scheme. The distribution of sea-level pressure in each case is specified following Holland's (1980) hurricane pressure profile (Eq. 1) assuming a central pressure of p_c=966 hPa, a center location at 17.4° N, 63.6° W, an ambient pressure of p_n=1010 hPa, a maximum surface wind speed of V_m= 48.9 m s^{-1},

and a radius of maximum surface wind R_m= 40 km (estimated from airborne radar). The bogus information extends out to a radius of 300 km. A control simulation is performed in which no bogus vortex is included in the initial conditions. Three experiments are conducted that vary the information assimilated into the model:

Exp.1: Similar to Zou and Xiao (1999), only bogus sea-level pressure data is assimilated into the mesoscale model, i.e., $J = J_1 + J_b$.

Exp.2: Only bogus wind data is assimilated into the mesoscale model, i.e., $J = J_2 + J_b$.

Exp.3: Both wind and sea-level pressure data are assimilated into the model, i.e., $J = J_1 + J_2 + J_b$.

In experiments 2 and 3, the surface wind is specified by the relationship in (2) and extended into the vertical according to (4) with the following vertical profile, $F(\sigma)$=1.0, 0.95, 0.85, 0.65, 0.35, 0.15 for σ = 0.9, 0.75, 0.5, 0.4, 0.3, 0.15, respectively, and 0 above 0.15.

Similar to Zou and Xiao (2000), the specified sea-level pressure information are assimilated every 5 min within a 30-min window. The wind information is assimilated every 10 min in this 30-min window. This method assumes that the tendencies of surface pressure and wind are near zero during this half hour. Zou and Xiao (2000) indicated that such constraints can be incorporated by adding a penalty term to the cost function (Zou et al. 1992, Zou et al. 1993).

a. Numerical Results

1) Initial Vortex

For the assimilation experiments, minimization of the cost function generally converges

in about 30 iterations. In order to compare the experiments equally, the minimization is stopped after 30 iterations for all experiments. During the minimization procedure, the assimilation variables (sea-level pressure and/or winds) are forced toward the bogus information, while all other variables (e.g., temperature and moisture) are free to develop in a model-consistent manner.

The improvement in the structure of the initial vortex is apparent after the assimilation procedure. Figure 2 shows the distribution of the initial sea-level pressure, wind speed and wind vectors at 850 hPa before (Fig. 2a) and after data assimilation (Figs. 2b-d). The vortices after variational data assimilation are more intense than the vortex in the global analysis. The winds show a more realistic distribution and maximum winds occur closer to the vortex center. Although a symmetric surface low (and/or wind field) is assimilated during the minimization procedure, the resulting wind speed distribution includes an asymmetric structure in all three assimilation experiments. A vortex flow is also generated above the surface for all experiments (e.g., Fig.4b).

In order to show that the proposed scheme produces initial fields that realistically resemble three-dimensional structures of hurricanes, we show the distributions of the zonal wind, meridional wind, potential temperature, and the water vapor mixing ratio through the center of the vortex prior to assimilation (Ctrl, Fig. 3) and after assimilation (Exp. 3, Fig. 4). Without the bogus vortex, the zonal and meridional flow patterns (Figs. 3a, b) indicate easterly flow across a broad, weak vortex. Potential temperature and moisture perturbations are small (Figs. 3c, d). In contrast, the initial vortex generated by the 4-D VAR technique reproduces many features of mature hurricanes, including low-level inflow and upper-level outflow (Fig. 4a) and a strong

tangential circulation (Fig. 4b). Although only bogus sea-level pressure and wind data were specified, the temperature and moisture fields are also adjusted with a warm core feature appearing during the assimilation process. Similar features for these fields are found in Exp. 1 and Exp. 2, but the amplitudes vary.

Significant differences are seen between the experiments in the vertical velocity fields (Fig. 5). In the absence of the bogus vortex, subsidence occurs in the area of the observed hurricane with very weak upward motion at larger radii. With assimilation of the sea-level pressure data only (Exp. 1, Fig. 5b), very strong upward vertical motion occurs near the hurricane center. This strong vertical motion decreases when the wind data are introduced in the assimilation process (e.g., Exp. 3, Fig. 5d). By assimilating wind data only, upward vertical motion appears strong only at upper levels. In each case, the strongest upward motions occur near the center of the storm, unlike observed vertical motions in hurricanes in which the upward motion is displaced from the center in the form of an eyewall. This simulated structure results from the fact that the 36-km horizontal grid spacing is incapable of resolving the eyewall and eye (in this case, the distance between one side of the eyewall, across the eye, to the other side is effectively three grid points). While the initial vertical motion structure is not fully adequate, the upward motions obtained from the forecast on the 12-km grid very rapidly shift away from the center to form a realistic looking eyewall (not shown). Thus, as will be shown in the next section, inadequacies in the initial vertical motions are not necessarily detrimental to the forecast.

2) Forecast Impacts

Figure 6 shows the simulated tracks compared to the observed track of Georges. All of the simulations produce tracks that are to the right of the observed motion. The two cases for

which bogus pressure fields are assimilated (Exp. 1 and Exp. 3) show improved skill over the control simulation and the case involving assimilated surface winds only (Exp. 2). Experiments 1 and 3 provide nearly a 30% improvement in the track forecast, but still lack a critical aspect of Georges development—its direct interaction with the orography of Puerto Rico and the Dominican Republic.

Figure 7 shows the temporal variations of the minimum sea-level pressure (or hurricane central pressure, Fig. 7a) and maximum winds at the lowest model level (Fig. 7b). The results suggest significant improvement in both the pressure and wind forecasts when bogus vortices are introduced into the initial conditions. However, there are marked differences between the experiments. In Exp. 1, in which only bogus pressure information was used, a dramatic spin down of the storm occurs within the first 6 h of the forecast, after which the case shows only marginal improvement over the control simulation. In Exp. 2, in which only bogus surface winds were used, the wind forecast is quite reasonable, but the minimum pressure time series suggests an inadequate adjustment of the initial pressure field and a subsequent pressure forecast that is often up to 10-20 hPa in error. Experiment 3, which uses both bogus pressure and wind information, provides the best forecast. The minimum central pressure and maximum winds are generally within 5-10 hPa and 5 m s^{-1}, respectively, of the observed values. In particular, note that the pressure rises and falls are comparable in behavior to the observed tendencies. While the observed movement of George over the island led to rapid weakening of the storm after 24 h, the more northward movement of the storm in Exp. 3 leads to less weakening.

The forecast results in experiments 1 and 2 indicate very different model responses to the separate assimilation of surface pressure and winds. Figure 8 shows the vector wind differences

between the experiments and the control simulation as well as the divergence field. When only bogus surface pressure information is simulated (Exp. 2), the response in the wind field is contained largely within the divergent component of the wind, with strong convergence leading to strong upward motion in the center, as noted in Fig. 5b. In contrast, assimilation of only the bogus surface wind information (which are non-divergent) leads to an expected dominance of the rotational component of the wind field and a weakly convergent flow near the eye. Only when both the bogus surface pressure and wind information are assimilated together does the model produce a strong rotational and convergent wind field.

The improvement of the forecast obtained by using bogus pressure and wind information is demonstrated in Fig. 9, which shows forecasted 6-h precipitation accumulation for the control case and Exp. 3. In the control simulation (Fig. 9a), the vortex is weak and light precipitation covers a broad area to the north and east of the center. In Exp. 3 (Fig. 9b), intense precipitation occurs on the eastern side of the vortex with much lighter precipitation on the western side. Outer convective bands are seen well to the east of the center. Figure 9c shows the distribution of radar reflectivity from the lower-fuselage radar of the National Oceanic and Atmospheric Administration (NOAA) WP-3D reconnaissance aircraft at 1742 UTC 21 September, approximately 18 min prior to the time of Fig. 9b. The radar data indicate a qualitatively similar distribution of precipitation, with maximum rainfall on the eastern side of the storm center. The results show that the assimilation of the bogus pressure and wind fields leads not only to adjustments to those particular fields in the initial conditions, but also to significant adjustments to other fields such as moisture. Furthermore, despite the assimilation of axisymmetric distributions of pressure and wind, realistic asymmetries are produced for this case by the 4-D

VAR system.

5. Effects of vortex size

In the previous experiments, the bogus vortex was specified according to the observed size of the hurricane with a radius of maximum winds comparable to the model grid spacing. In this section, we explore the sensitivity of the assimilation and forecast to the size of the bogus vortex by specifying a vortex that is resolved better by the 36-km grid spacing. Two experiments are performed.

Exp. 4: Same as Exp. 1, except the radius of maximum winds is set to 120 km, instead of 40 km.

Exp. 5: Same as Exp. 3, except the radius of maximum winds is set to 120 km.

Similar to experiments 1 and 3, reasonable initial vortex structures appear after data assimilation in experiments 4 and 5. To illustrate the changes caused by the increased size of the vortex, Fig. 10 compares the wind speed for experiments 3 and 5. In Exp. 3 (Fig. 10a), the radius of maximum winds is small and the model is unable to resolve the weak horizontal motions that should be present in the eye. In contrast, in Exp. 5 (Fig. 10b), the vortex is sufficiently large that the wind speed minimum in the eye is resolved.

Comparison of the vertical motions in Exp. 4 (Fig. 11a) with Exp. 1 (Fig. 5b) shows that even with the larger vortex, assimilation of pressure information only leads to strong upward motion near the center. In contrast, Fig. 11b shows that assimilation of both pressure and wind information associated with the larger vortex results in weaker vertical motion. In Exp. 3 (Fig. 5d), the upward motion was strongest near the center, which was attributed to inadequate

horizontal resolution. In Exp. 5 (Fig. 11b), upward motion is located to the east of the center with a suggestion of weak upward motion to the west and weak downward motion near the center below 350 hPa. Thus, when the vortex is sufficiently large for it to be resolved on the horizontal grid, more reasonable vertical motion patterns are obtained.

The impact of vortex size on forecasts of track and intensity are shown in Figs. 12 and 13. The simulated intensity in Exp. 4 is slightly better than in Exp. 1, but similar to Exp. 1, the initial vortex spins down very quickly at the beginning of the forecast integration (Fig. 13). The results for Exp. 5 show that both the track and intensity forecasts are improved tremendously. In particular, about 70% of the track error is reduced (Fig. 12) and the intensity forecast catches most features of the observed intensity changes. The two landfalls of Hurricane Georges during this period are well predicted. The temporal variations of central sea-level pressure agree well with the observations (Fig. 13a) except for showing less of a rise in the final 12 h. This error may be due to the lack of high-resolution terrain information in the model. The forecast impacts suggest that using a vortex that is larger than observed may not be detrimental to the simulation, but in fact can provide improved results as the vortex is resolved better on the model horizontal grid.

6. Hurricane Bonnie (1998)

The experiments for Hurricane Georges show that the bogus vortex technique can work well for a relatively steady hurricane, but how well can it work for rapidly deepening storms? In this section, the bogusing technique is applied to the case of Hurricane Bonnie (1998) just prior to its rapid intensification. Bonnie became a hurricane around 0000 UTC 22 August 1998. By

0600 UTC, reconnaissance aircraft detected a nearly complete eyewall and flight-level winds up to 39 m s^{-1}. Over the next two days, Bonnie moved northwestward (Fig. 14) and developed maximum winds of 51 m s^{-1} and a minimum pressure of 954 hPa.

Because of our interest in the rapid deepening of the hurricane, 0000 UTC 22 August is selected as the initial time for simulation. The experiment configuration is similar to Exp. 5 for Hurricane George in which both bogus surface pressure and wind information are assimilated for a vortex with radius of maximum winds of 120 km. The model includes an outer domain with 36-km grid spacing (domain C in Fig. 14) and a movable, nested domain with 12 km grid spacing (domain D in Fig. 14). Assimilation of the bogus vortex is performed only for the 36-km domain while initial conditions for the 12-km grid are interpolated from the coarser domain. The parameters defining the bogus vortex are the follows: p_c=991 hPa at the hurricane center (21.1° N, 67.3° W), p_n=1012 hPa, V_m= 33.5 m s^{-1}, and R_m=120 km. The bogus information extends out to a radius of 300 km.

Two experiments are conducted, one without (Ctrl) and one with (Exp. 6) the bogus vortex. Assimilation of the bogus vortex information is stopped after 30 iterations. Figure 15 shows the simulated tracks compared to the observed track of Bonnie. Without the bogus vortex, the control experiment shows significant errors in the initial position of the storm and a much too rapid movement to the northwest. Assimilation of the bogus information corrects the initial position error, reduces the subsequent track error, and even captures some of the slowing down of the storm late in the forecast period.

Figure 16 shows the temporal variations of the minimum sea-level pressure (Fig. 16a) and maximum wind at the lowest model level (Fig. 16b). Clearly, with assimilation of the bogus

vortex, the simulation is better able to reproduce the reduction of the central pressure and increase of surface wind speed. However, the simulated intensification is slower than observed. This result suggests that, in addition to possible deficiencies in the model physics, the inability of the model to exactly capture the very rapid intensification of Bonnie may be the result of inadequacies in the synoptic-scale conditions or the mesoscale structure of the initial vortex and highlights the potential role that satellite remotely sensed data can play in improving hurricane forecasts. Assimilation of cloud and vapor tracked winds and precipitable water from geostationary satellites may provide improvements to synoptic-scale fields while rainfall information from the Special Sensor Microwave/Imager (SSM/I) and Tropical Rainfall Measuring Mission (TRMM) satellites offer potential improvements to mesoscale structure.

The contribution of the bogus vortex to the simulated precipitation is indicated in Fig. 17, which shows the forecasted 6-h accumulated precipitation at 2000 UTC 23 August (hour 44 of the forecast) for the control case and Exp. 6. A corresponding radar reflectivity pattern for the period 1950-2018 UTC from NOAA reconnaissance aircraft is shown in Fig. 17c. Both the control forecast and Exp. 6 develop heavy precipitation on the eastern side of the storm, comparable to observations. In the control forecast, the heavy precipitation is located approximately 2° of longitude away from the center while for Exp. 6, the heavy precipitation is within 1° longitude of the center, in much better agreement with observations.

7. Conclusions

The effectiveness of 4-D VAR techniques for creating "bogus" vortices in numerical simulations of hurricanes is examined by using the Penn State/NCAR nonhydrostatic mesoscale

model (MM5) and its adjoint system. The variational bogus vortex scheme is applied to simulations of Hurricane Georges (1998) using three different methodologies: 1) assimilation of bogus sea-level pressure information only, 2) assimilation of bogus wind data only, and 3) assimilation of both bogus wind and surface pressure data. The bogus vortex data are assimilated within a 30-min assimilation window in order to generate the initial vortex for subsequent forecasts. The experiments suggest that assimilation of both pressure and wind information provides the best results. With assimilation of sea-level pressure data only, the response of the horizontal wind field is dominated by the divergent component of the wind such that the model generates an initial vortex with very strong upward vertical motion at the center. The intensity of this vortex decreases very rapidly within the first 6 h of the simulation. With assimilation of the wind data only, the response of the horizontal wind field is dominated by the rotational component of the wind and vertical motions near the center are significantly reduced. However, the adjustment of the pressure field is inadequate and contributes to a poor forecast of storm intensity. With assimilation of both pressure and wind data, the response of the wind field contains both strong rotational and divergent components. The central pressure and maximum wind forecasts are in good agreement with observations.

During the data assimilation period, even though only sea-level pressure and/or wind information is included, other prognostic variables such as temperature and moisture are adjusted in a manner consistent with the model resolution and physics. The vortex generated by the 4-D VAR technique reproduces many of the structural features of hurricanes including radial inflow and outflow and the warm core. The pattern of forecasted 6-h accumulated rainfall derived from the bogus vortex is in good agreement with radar observations, indicating a reasonable

Acknowledgments: The authors wish to express their gratitude to Dr. Xiaolei Zou of Florida State University for her encouragement and for providing the MM5 adjoint code used in this study and also to Drs. Wei-Kuo Tao and Robert F. Adler of NASA/GSFC and Dr. Ramesh Kakar of NASA/HQ for their support of this research. Computing resources were provided by NASA Goddard Space Flight Center.

References

Anthes, R. A. 1982: Tropical Cyclones: Their Evolution, Structure and Effects. American Meteorological Society. 208 pp.

Bender, M. A., R. J. Ross, R. E. Tuleya and Y. Kurihar, 1993: Improvements in tropic cyclone track and intensity forecasts using the GFDL initialization system. *Mon. Wea. Rev.*, **121**, 2046-2061

Blackadar, A. K., 1976: Modelng the nocturnal boundary layer. *Preprints, Third Symp. on Atmospheric Turbulence, Diffusion, and Air Quality*, Raleigh, Amer. Meteor. Soc., 46-49.

———, 1979: High resolution models of the planetary boundary layer. *Advances in Environmental Science and Engineering*, Vol. 1, No. 1, J. Pfafflin and E. Ziegler, Eds., Gordon and Breach, 50-85.

Dudhia, J., 1993: A nonhydrostatic version of the Penn State-NCAR mesoscale model: Validation tests and simulation of an Atlantic cyclone and cold front. *Mon. Wea. Rev.*, **121**, 1493-1513

Grell, G. A., J. Dudhia, and D. R. Stauffer, 1995: A description of the fifth-generation Penn State/ NCAR mesoscale model (MM5). NCAR Technical Note, NCAR/TN-398 + STR, 138 pp. [Available from NCAR Publications Office, P. O. Box 3000, Boulder, CO 80307-3000].

Holland, G. 1980: An analytic model of the wind and pressure profile in hurricanes. *Mon. Wea. Rev.*, **108**, 1212-1218

Iwasaki, T., H. Nakano, and M. Sugi, 1987: The performance of a typhoon track prediction model with cumulus parameterization. *J. Meteor. Soc. Japan*, **65**, 555-570

Kuo, Y.-H., and X. Zou, and Y. R. Guo, 1996: Variational assimilation of precipitable water

using a nonhydrostatic mesoscale adjoint model. Part I: Moisture retrieval and sensitivity experiments. *Mon. Wea. Rev.*, **124**, 122-147.

Kurihara, Y., M. A. Bender, and R. J. Ross, 1993: An initialization scheme of hurricane models by vortex specification. *Mon. Wea. Rev.*, **121**, 2030-2045

Kurihara, Y., M. A. Bender, R. E. Tuleya, and R. J. Ross, 1990: Prediction experiments of Hurricane Gloria (1985) using a multiply nested movable mesh model. *Mon. Wea. Rev.*, **118**, 2185-2198.

Leslie, L. M., and G. J. Holland, 1995: On the bogussing of tropical cyclones in numerical models: A comparison of vortex profiles. *Meteorol. Atmos. Phys.*, **56**, 101-110.

Lord, S. J., 1991: A bogusing system for vortex circulations in the National Meteorological Center global forecast model. The 19th Conference on Hurricane and Tropical Meteorology, American Meteorological Society, 6-10 May, 1991, Miami, Florida. 328-330.

Manning, K. W., and P. L. Haagenson, 1992: Data ingest and objective analysis for the PSU/NCAR modeling system: Programs DATAGRID and RAWINS. NCAR Technical Note (NCAR/TN-376+IA), 209 pp. [Available from NCAR Publications Office, P. O. Box 3000, Boulder, CO 80307-3000]

Mathur, M. B., 1991: The National Meteorological Center's quasi-Lagrangian model for hurricane prediction. *Mon. Wea. Rev.*, **119**, 1419-1447

Smolarkiewicz, P. K., and G. A. Grell, 1992: A class of monotone interpolation schemes. *J. Comp. Phys.*, **101**, 431-440.

Trinh, Van Thu and T. N. Krishnamuti, 1992: Vortex initialization for Typhoon track prediction. *Meteorol. Atmos. Phys.*, **47**, 117-126.

Zhang, D.-L., and R. A. Anthes, 1982: A high-resolution model of the planetary boundary layer — Sensitivity tests and comparisons with SESAME-79 data. *J. Appl. Meteor.*, **21**, 1594-1609.

Zou, X. and Q. Xiao, 2000: Studies on the initialization and simulation of a mature hurricane using a variational bogus data assimilation scheme. *J. Atmos. Sci.* (in press).

Zou, X., W. Huang and Q. Xiao, 1998: A user's guide to the MM5 adjoint modeling system. NCAR TN-437+IA. MMM division, NCAR. [Available from NCAR Publications Office, P. O. Box 3000, Boulder, CO 80307-3000].

Zou, X., Y.-H. Kuo and Y.-R. Guo, 1995: Assimilation of atmospheric radio refractivity using a nonhydrostatic adjoint model. *Mon. Wea. Rev.*, **123**, 2229-2249.

Zou, X., I. M. Navon and J. Sela 1993: Control of gravity oscillations in variational data assimilation. *Mon. Wea. Rev.*, **121**, 272-289.

Zou, X., I. M. Navon, and F. X. Le Dimet, 1992: Incomplete observations and control of gravity waves in variational data assimilation. *Tellus*, **44A**, 273-296

Figure Captions

Figure 1. Location of the model domains for Hurricane Georges (1998). Domain A is the 36-km grid and domain B is the nested, 12-km grid used in the forecast. Domain B is moved during the simulation from B1 to B2. Estimates of the center location at 6-h intervals from the Hurricane Research Division (HRD) of NOAA are marked by circles. The period included in the simulation is marked by the bold segment of the track.

Figure 2. Distributions of the sea-level pressure (thin dashed line, 4 mb interval), horizontal wind vectors and wind speed (thick solid line, 5 m s^{-1} interval) at 850 hPa at the end of the assimilation window (30 min). a) ECMWF analysis without the bogus vortex (Ctrl), b) assimilation of surface pressure only (Exp. 1), c) assimilation of wind data only (Exp. 2), and d) assimilation of both pressure and wind data (Exp. 3).

Figure 3. East-west cross sections through the center of the vortex (17.4° N, 63.6° W) at 30 min for the control run. a) Zonal wind (u, 2.5 m s^{-1} contour interval), b) meridional wind (v, 5 m s^{-1} interval), c) potential temperature (θ, 4 K interval), and d) water vapor mixing ratio (q_v, 2 g kg^{-1} interval).

Figure 4. Same as Figure 3, but for Exp. 3.

Figure 5. East-west cross sections of vertical velocity through the center of vortex (17.4° N, 63.6° W) at 30 min for a) ECMWF analysis, b) Exp. 1, c) Exp. 2, and d) Exp. 3. The contour interval is 2.5 cm s^{-1} for (a) and 50 cm s^{-1} for (b-d).

Figure 6. Forecasts of hurricane track for the control run and experiments 1-3 compared to the observed track. Center locations along the tracks are indicated every 6 hours.

Figure 7. Time series (at 6-hour intervals) of a) minimum sea-level pressure (hPa) and b) maximum winds (m s^{-1}) at the lowest model level (σ=0.995, approximately 50 m).

Figure 8. Vector wind differences between the control simulation and experiments 1-3 at 850 hPa, for (a) Exp. 1, (b) Exp. 2, and (c) Exp. 3. The shading indicates horizontal divergence with light shading indicating values less than -10^{-4} s^{-1} and dark shading indicating values less than -6×10^{-4} s^{-1}.

Figure 9. Accumulated rainfall (shaded contours), sea-level pressure (solid line, contour interval 4 hPa) and wind vectors at lowest σ level at 6 h into the forecast valid at 1800 UTC 21 September for a) the control simulation and b) Exp. 3. c) Radar reflectivity pattern from the lower fuselage of the NOAA P-3 reconnaissance aircraft valid at 1754 UTC 21 September.

Figure 10. East-west cross sections of wind speed through the center of vortex (17.4° N, 63.6° W) at the end of the assimilation window (30 min) for a) Exp. 3 and b) Exp. 5. The contour interval is 5 m s^{-1}.

Figure 11. East-west cross sections of vertical velocity through the center of vortex (17.4° N, 63.6° W) at the end of the assimilation window (30 min) for a) Exp. 3 and b) Exp. 5. The contour interval is 50 cm s^{-1}.

Figure 12. Forecasts of hurricane track for the control run and experiments 4 and 5 compared to the observed track. Center locations along the tracks are indicated every 6 hours.

Figure 13. Time series (at 6-hour intervals) of a) minimum sea-level pressure (hPa) and b) maximum winds (m s^{-1}) at the lowest model level (σ=0.995, approximately 50 m). Experiments 1 and 4 involve assimilation of sea-level pressure data only, while experiments 3 and 5 involve assimilation of both pressure and winds.

Figure 14. Location of the model domains for the simulation of Hurricane Bonnie (1998). Domain C is the 36-km grid and domain D is the nested 12-km grid used in the forecast. Domain D is moved during the simulation from D1 to D2. Estimates of the center location at 6-h intervals are marked by circles. The minimum sea-level pressure (hPa) and maximum surface wind (m s^{-1}) are show inside the brackets. The period included in the simulation is marked by the bold segment of the track.

Figure 15. Forecasts of hurricane track for the control run and Exp. 6 compared to the observed track. Center locations along the tracks are indicated every 6 hours.

Figure 16. Time series (at 6-hour intervals) of a) minimum sea-level pressure (hPa) and b) maximum winds (m s^{-1}) at the lowest model level (σ=0.995, approximately 50 m) for control simulation and Exp. 6 compared to obserations.

Figure 17. Six hour accumulated rainfall (shaded contours), sea-level pressure (solid line, contour interval 4 hPa) and wind vectors at lowest σ level at 44 h into the forecast valid at 2000 UTC 23 August for a) the control simulation and b) Exp. 6. c) Radar reflectivity pattern from the lower fuselage of the NOAA P-3 reconnaissance aircraft valid at 1956 UTC 23 August.

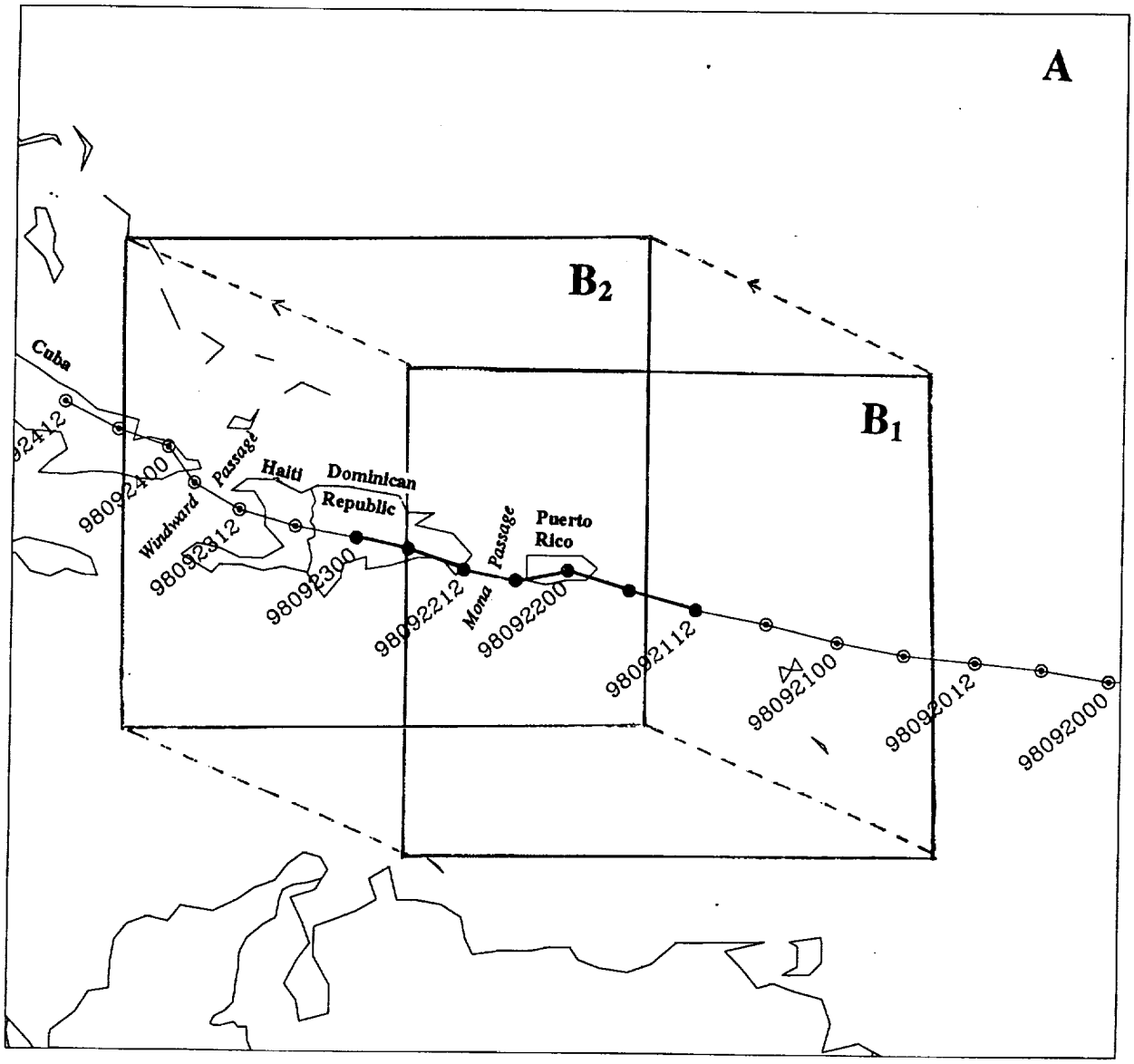
A
B2
B1
Cuba
Haiti
Dominican Republic
Windward Passage
Mona Passage
Puerto Rico
98092412
98092400
98092312
98092300
98092212
98092200
98092112
98092100
98092012
98092000

Fig. 1

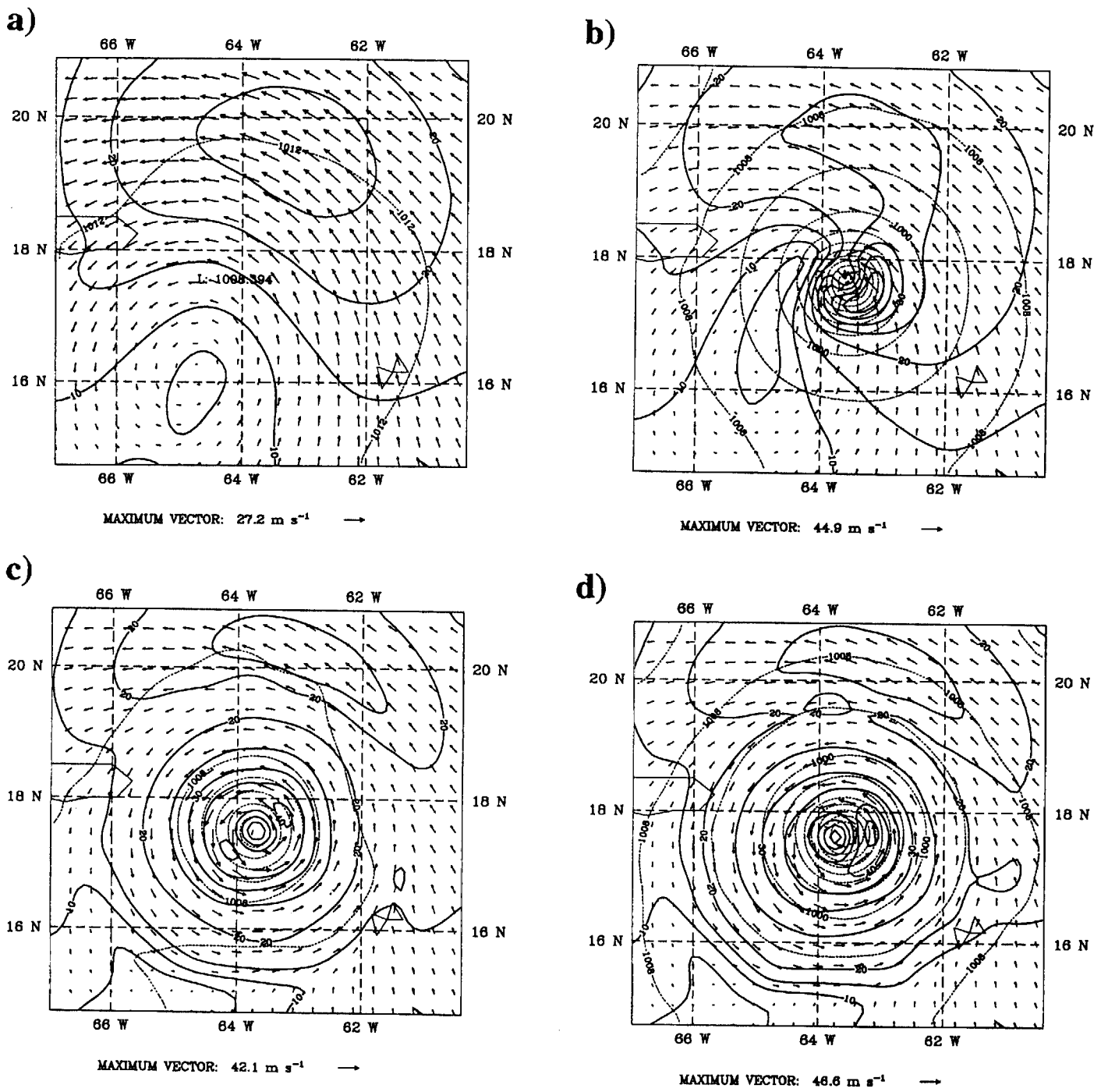
a)
66 W
64 W
62 W
20 N
18 N
16 N
L: 1008.394
MAXIMUM VECTOR: 27.2 m s⁻¹
b)
MAXIMUM VECTOR: 44.9 m s⁻¹
c)
MAXIMUM VECTOR: 42.1 m s⁻¹
d)
MAXIMUM VECTOR: 46.6 m s⁻¹

Fig. 2

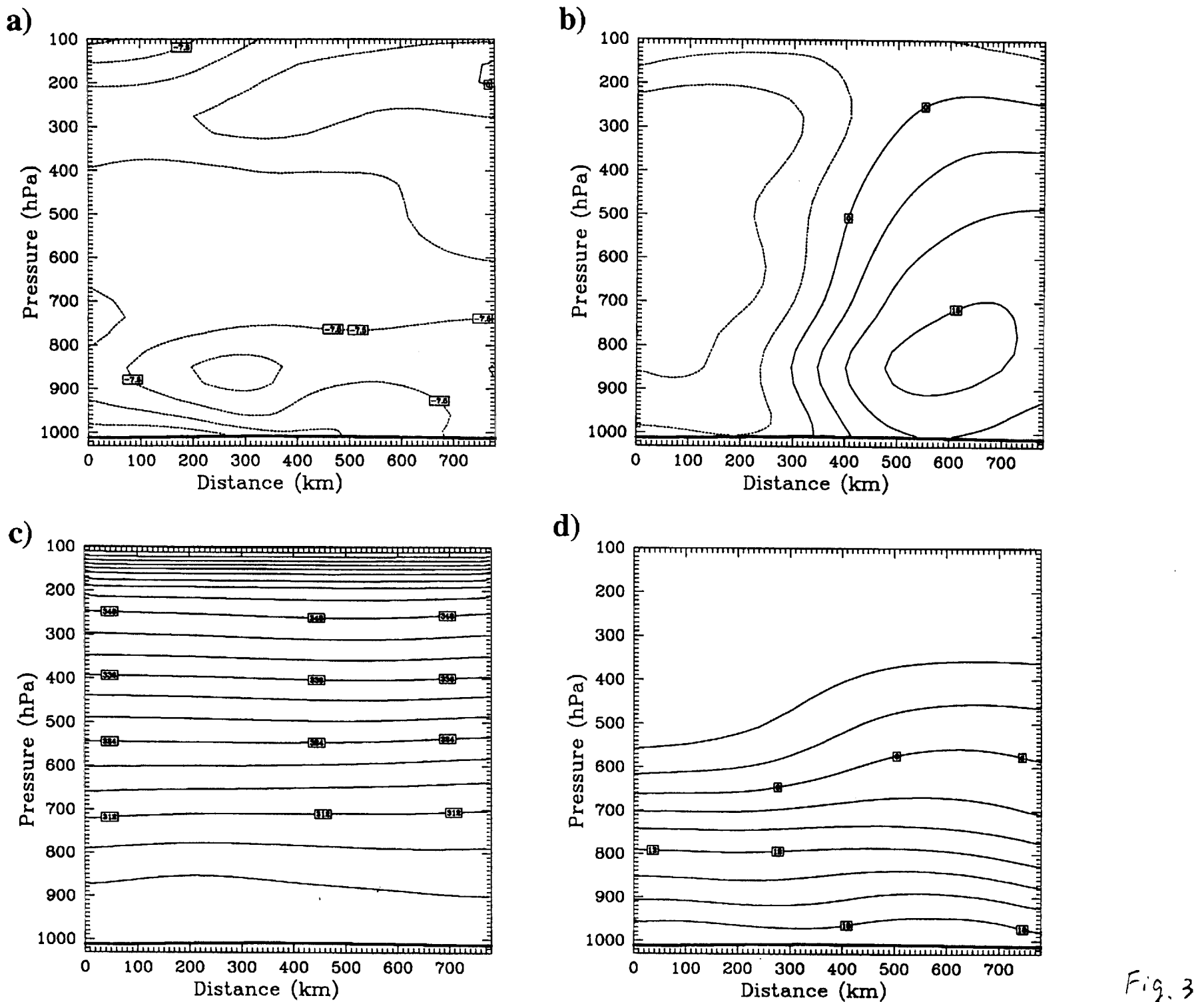
a)
b)
c)
d)
Pressure (hPa)
Distance (km)
100
200
300
400
500
600
700
800
900
1000
0
100
200
300
400
500
600
700

Fig. 3

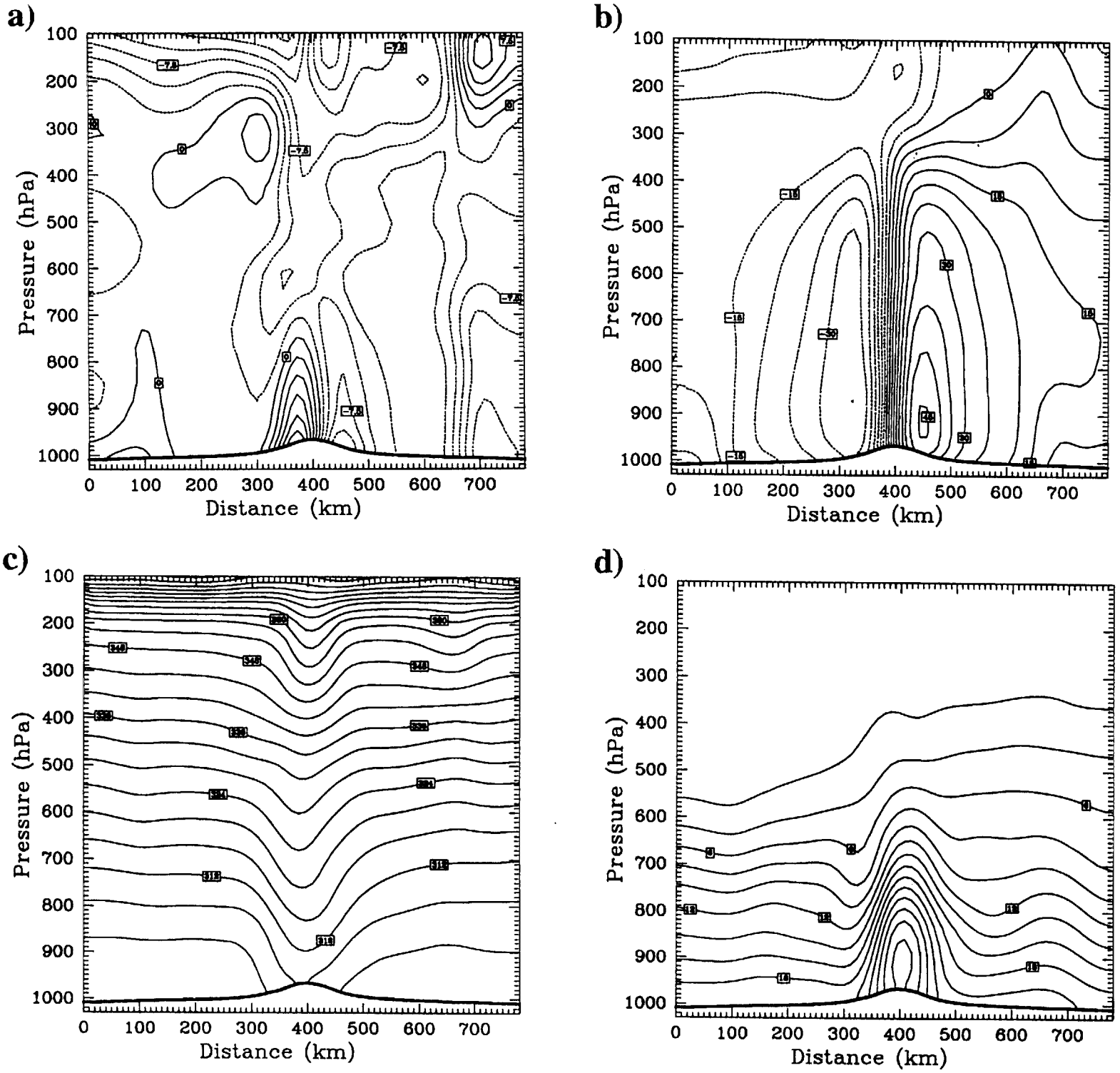
a)
b)
c)
d)
Pressure (hPa)
Distance (km)
100
200
300
400
500
600
700
800
900
1000
0
100
200
300
400
500
600
700

Fig. 4

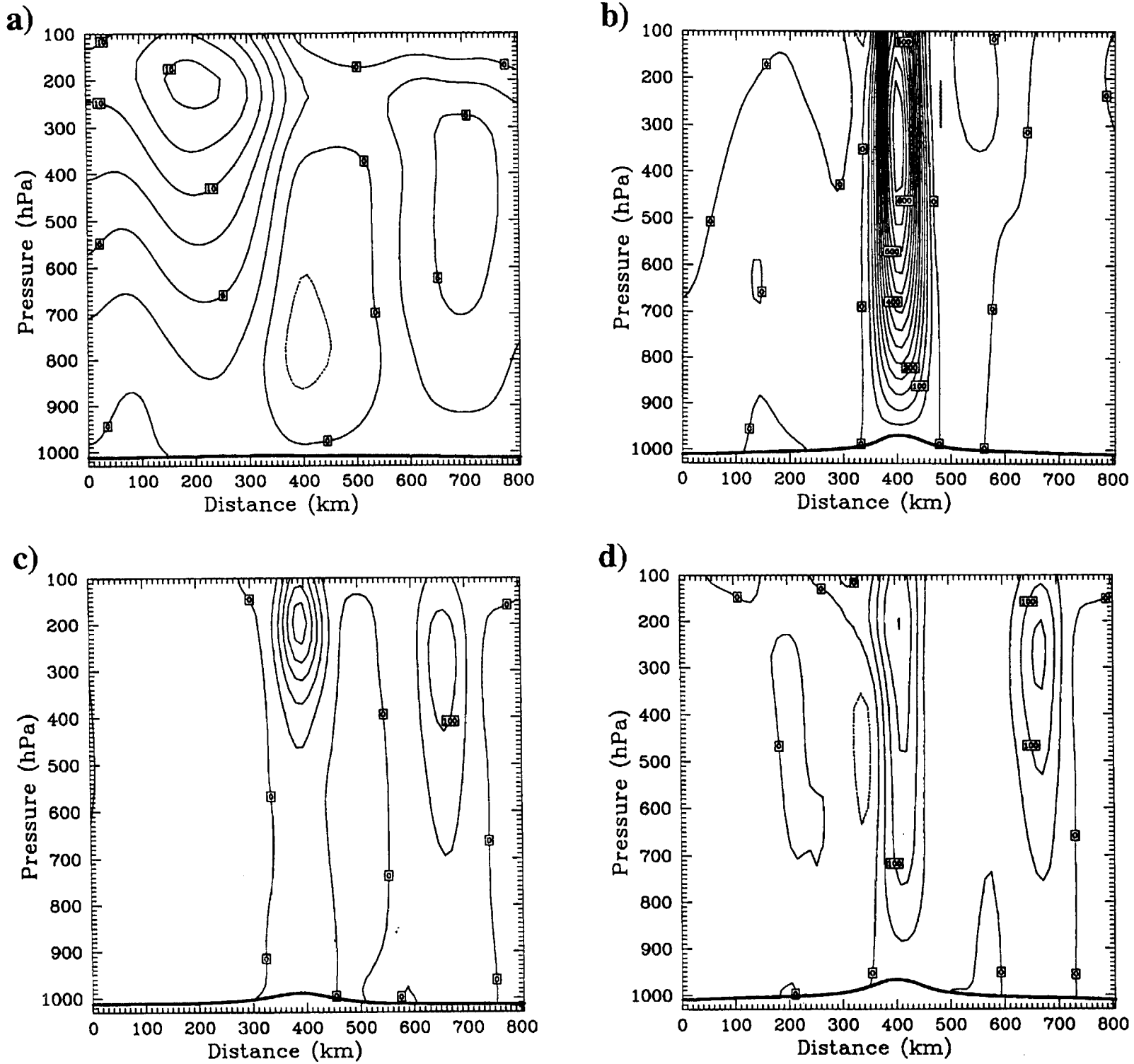
a)
b)
c)
d)
Pressure (hPa)
Distance (km)
100
200
300
400
500
600
700
800
900
1000
0
100
200
300
400
500
600
700
800

Fig. 5

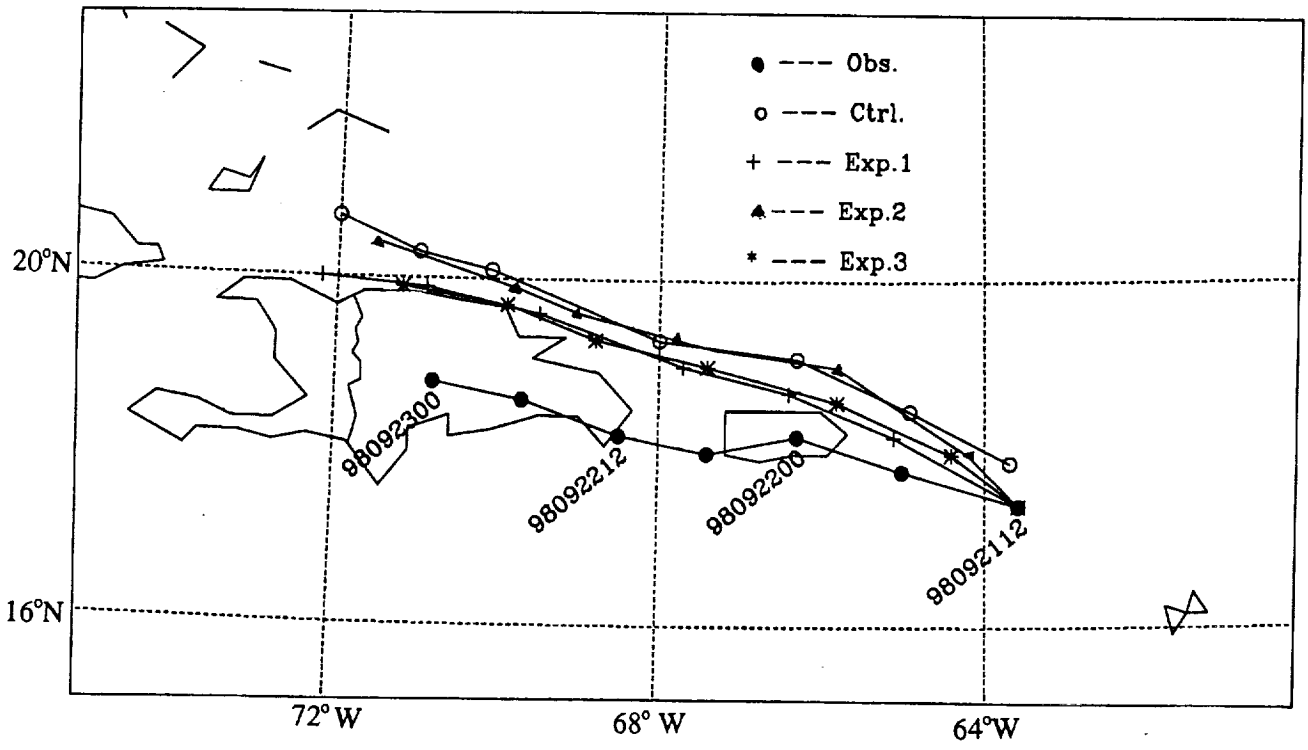
Obs.
Ctrl.
Exp.1
Exp.2
Exp.3
20°N
16°N
72° W
68° W
64°W
98092300
98092212
98092200
98092112

Fig. 6

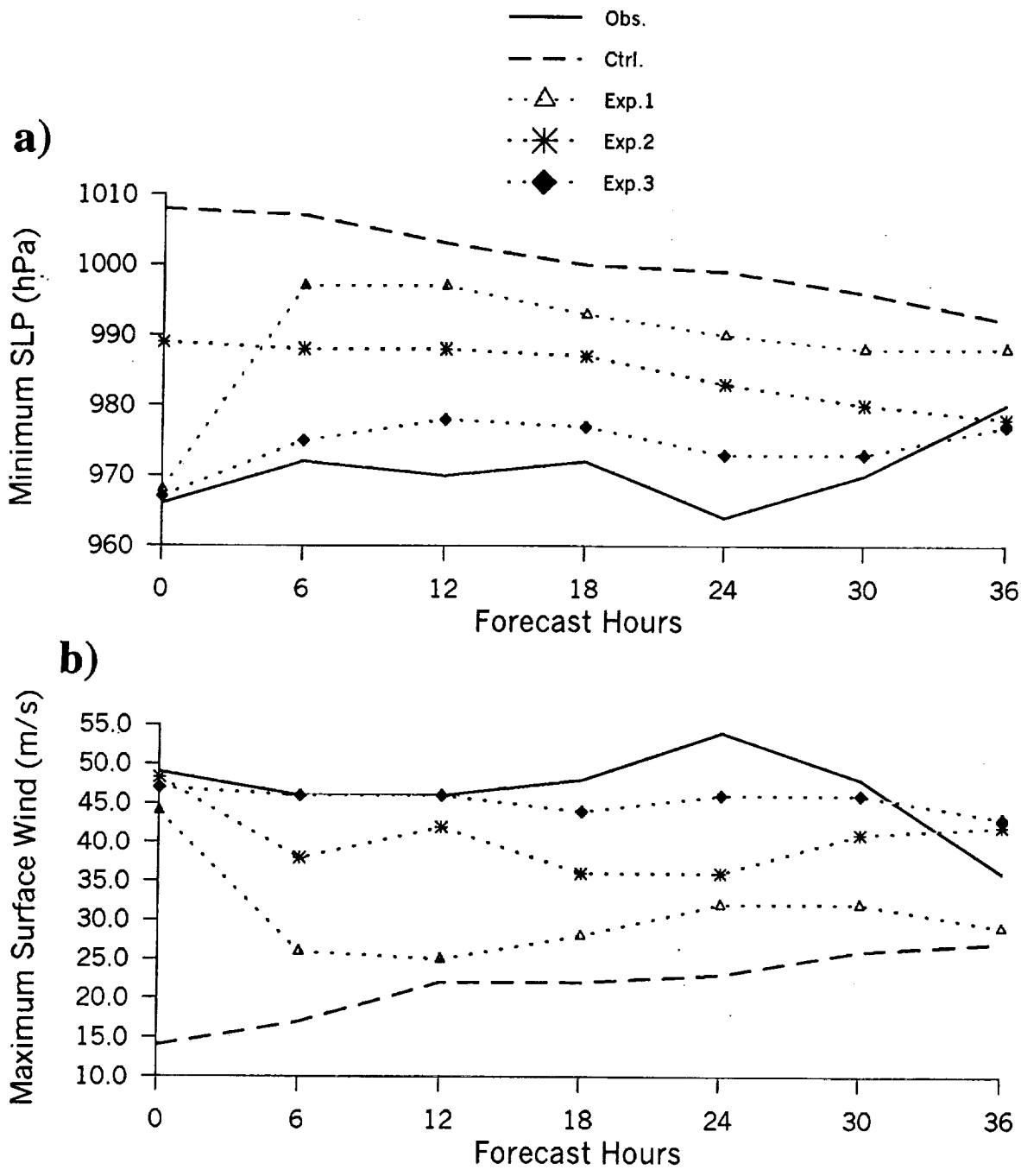
a)
Obs.
Ctrl.
Exp.1
Exp.2
Exp.3
Minimum SLP (hPa)
1010
1000
990
980
970
960
0
6
12
18
24
30
36
Forecast Hours
b)
Maximum Surface Wind (m/s)
55.0
50.0
45.0
40.0
35.0
30.0
25.0
20.0
15.0
10.0
0
6
12
18
24
30
36
Forecast Hours

Fig. 7

a)

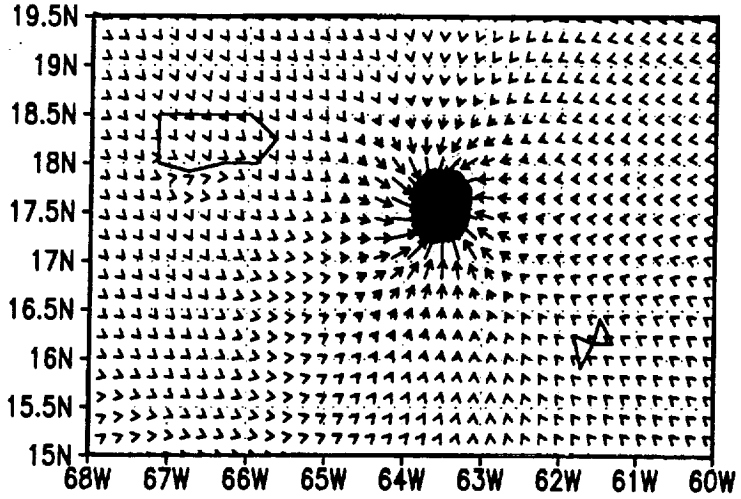

50

b)

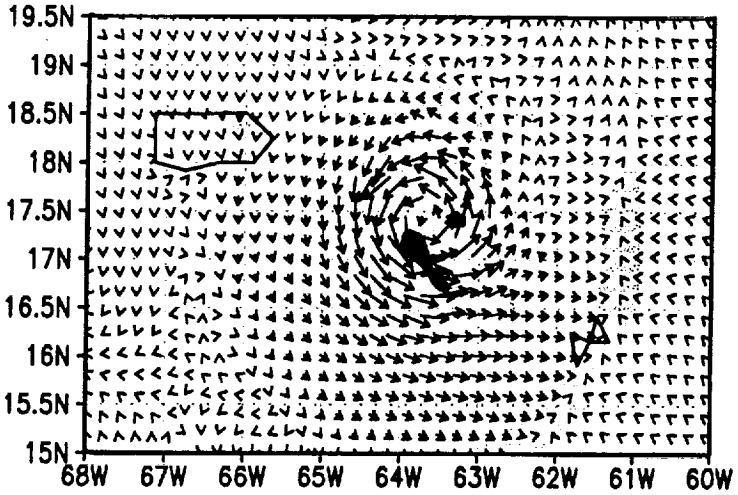

50

c)

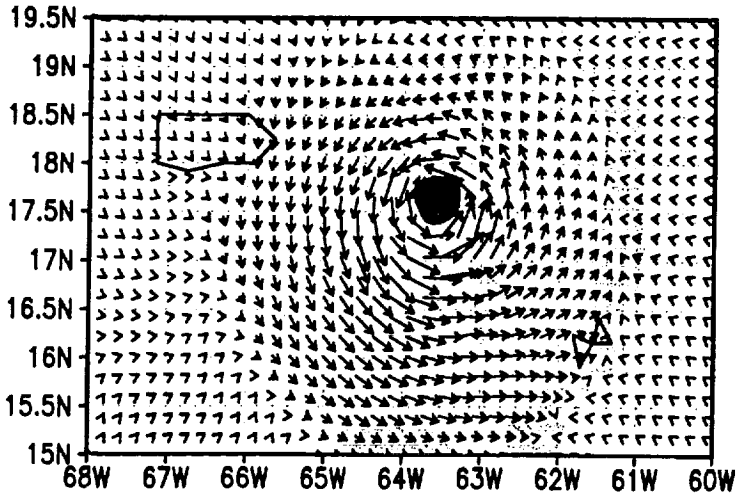

50

Fig. 8

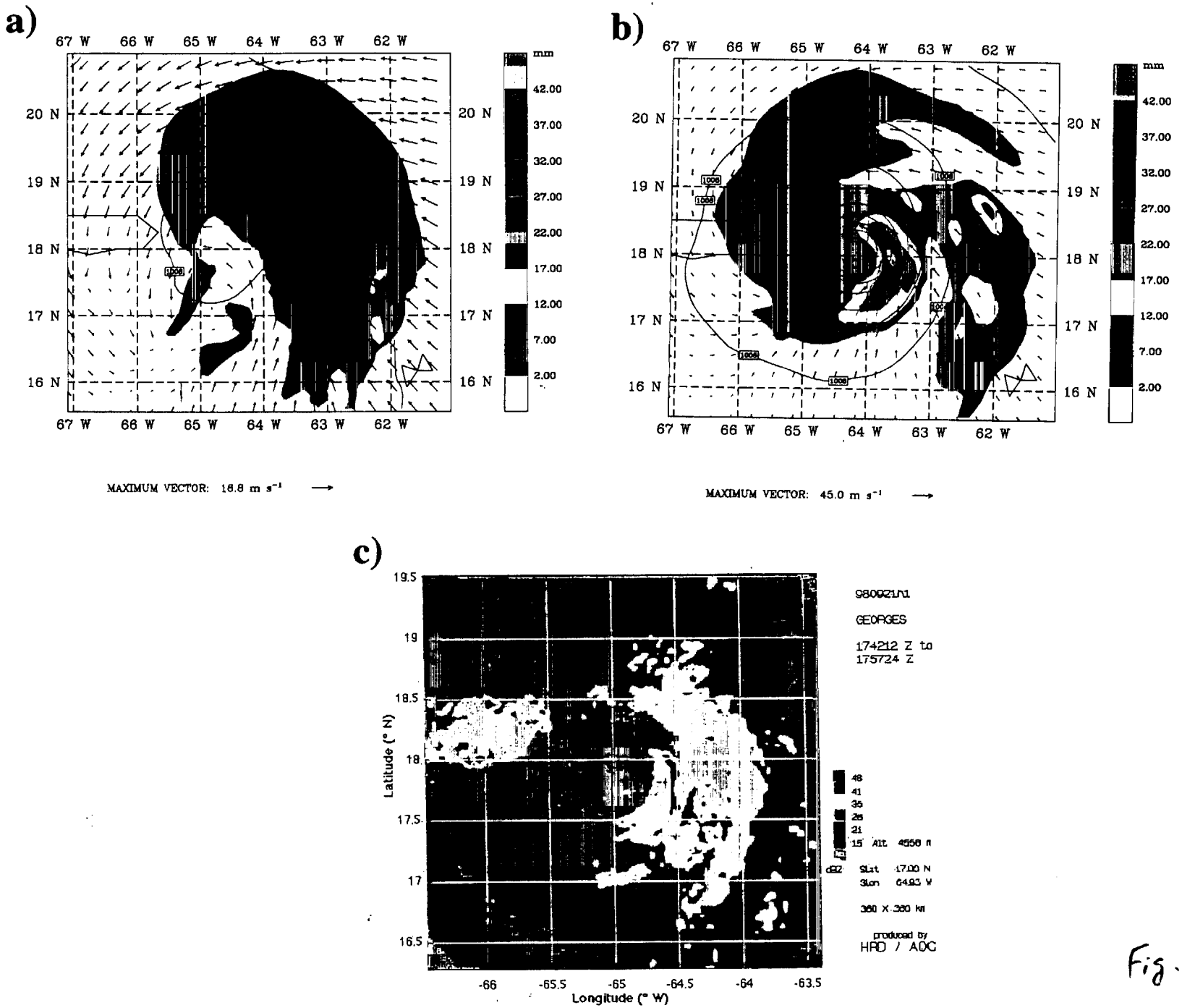
a)
67 W
66 W
65 W
64 W
63 W
62 W
20 N
19 N
18 N
17 N
16 N
mm
42.00
37.00
32.00
27.00
22.00
17.00
12.00
7.00
2.00
1008
MAXIMUM VECTOR: 18.8 m s-1
b)
MAXIMUM VECTOR: 45.0 m s-1
c)
980921h1
GEORGES
174212 Z to
175724 Z
Latitude (° N)
Longitude (° W)
19.5
19
18.5
18
17.5
17
16.5
-66
-65.5
-65
-64.5
-64
-63.5
48
41
35
28
21
15
dBZ
Alt 4556 ft
Slat 17.00 N
Slon 64.93 W
360 X 360 km
produced by
HRD / AOC

Fig. 9

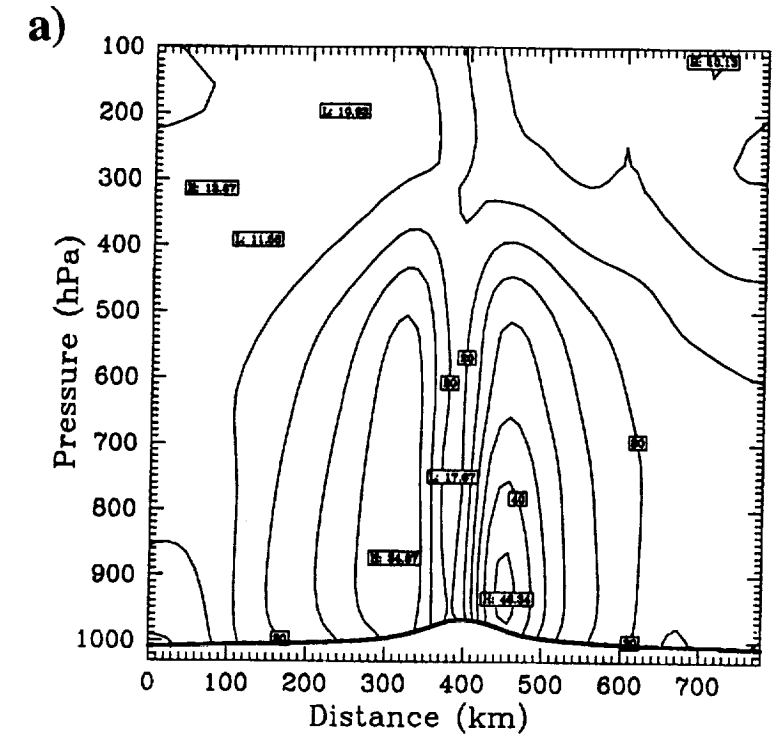
a)
Pressure (hPa)
100
200
300
400
500
600
700
800
900
1000
0
100
200
300
400
500
600
700
Distance (km)

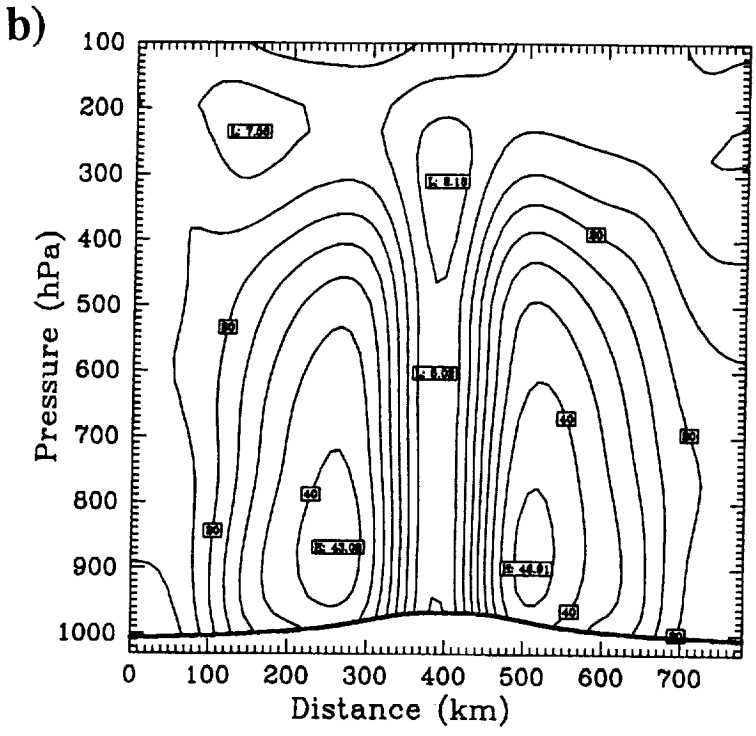
b)
Pressure (hPa)
100
200
300
400
500
600
700
800
900
1000
0
100
200
300
400
500
600
700
Distance (km)

Fig. 10

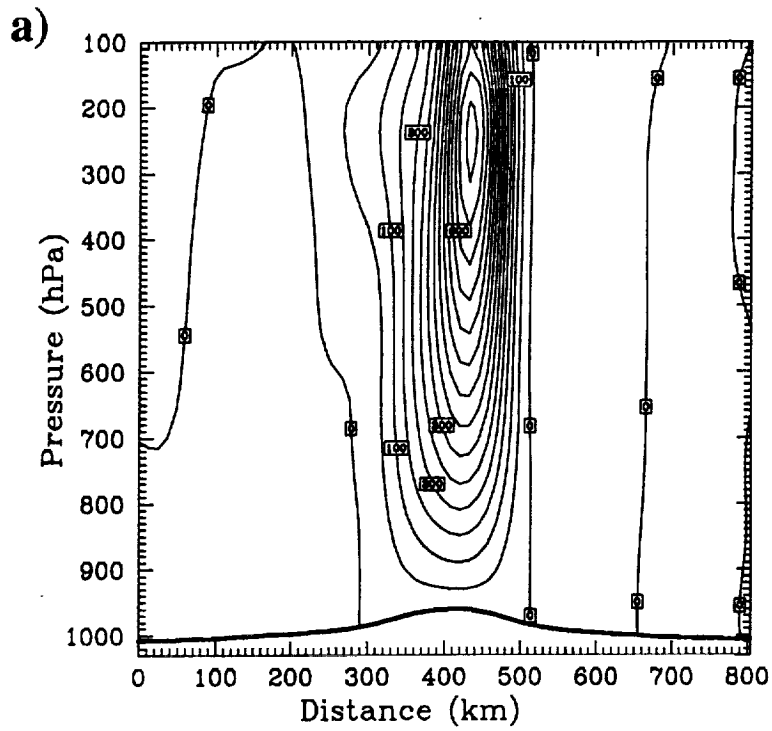
a)
Pressure (hPa)
100
200
300
400
500
600
700
800
900
1000
0
100
200
300
400
500
600
700
800
Distance (km)

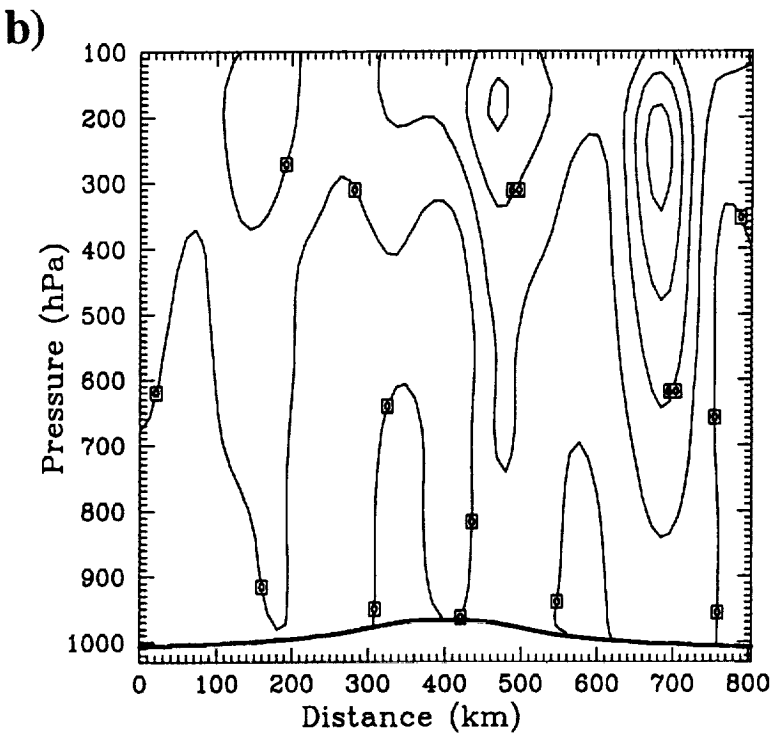
b)
Pressure (hPa)
100
200
300
400
500
600
700
800
900
1000
0
100
200
300
400
500
600
700
800
Distance (km)

Fig. 11

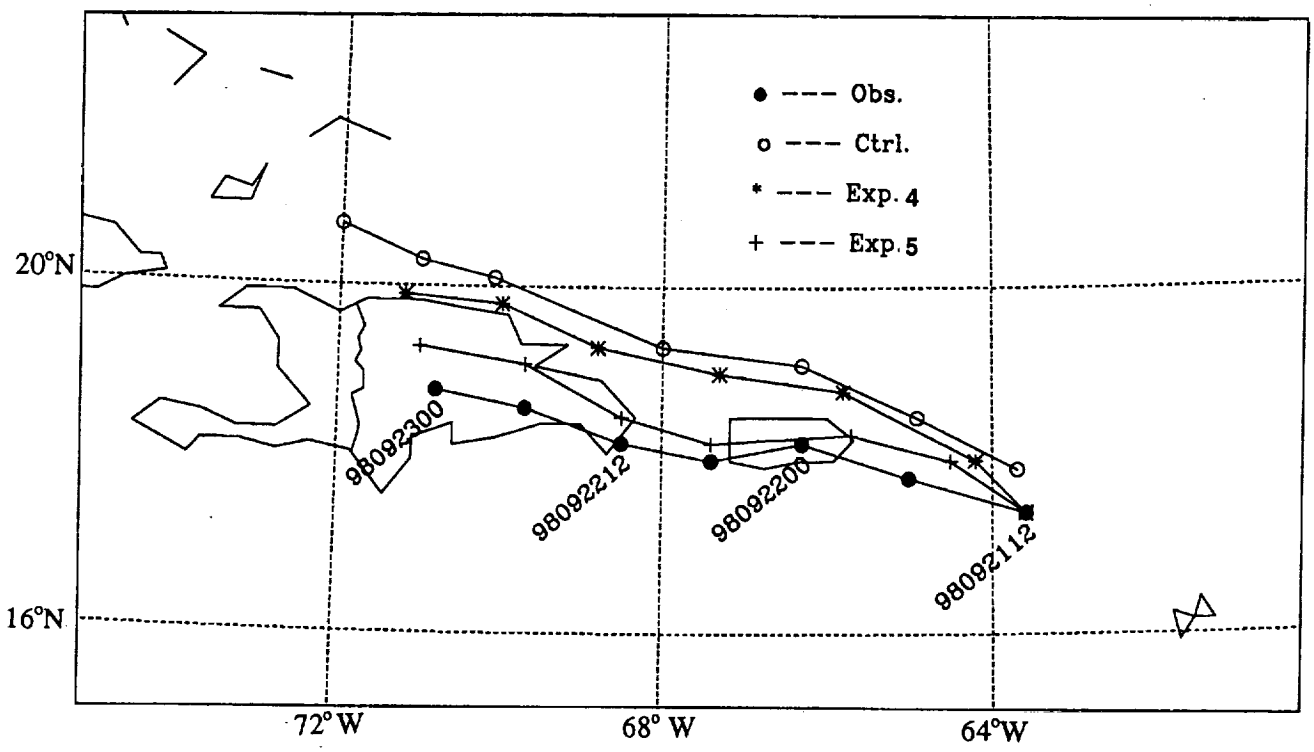
Obs.
Ctrl.
Exp. 4
Exp. 5
20°N
16°N
72° W
68° W
64°W
98092300
98092212
98092200
98092112

Fig. 12

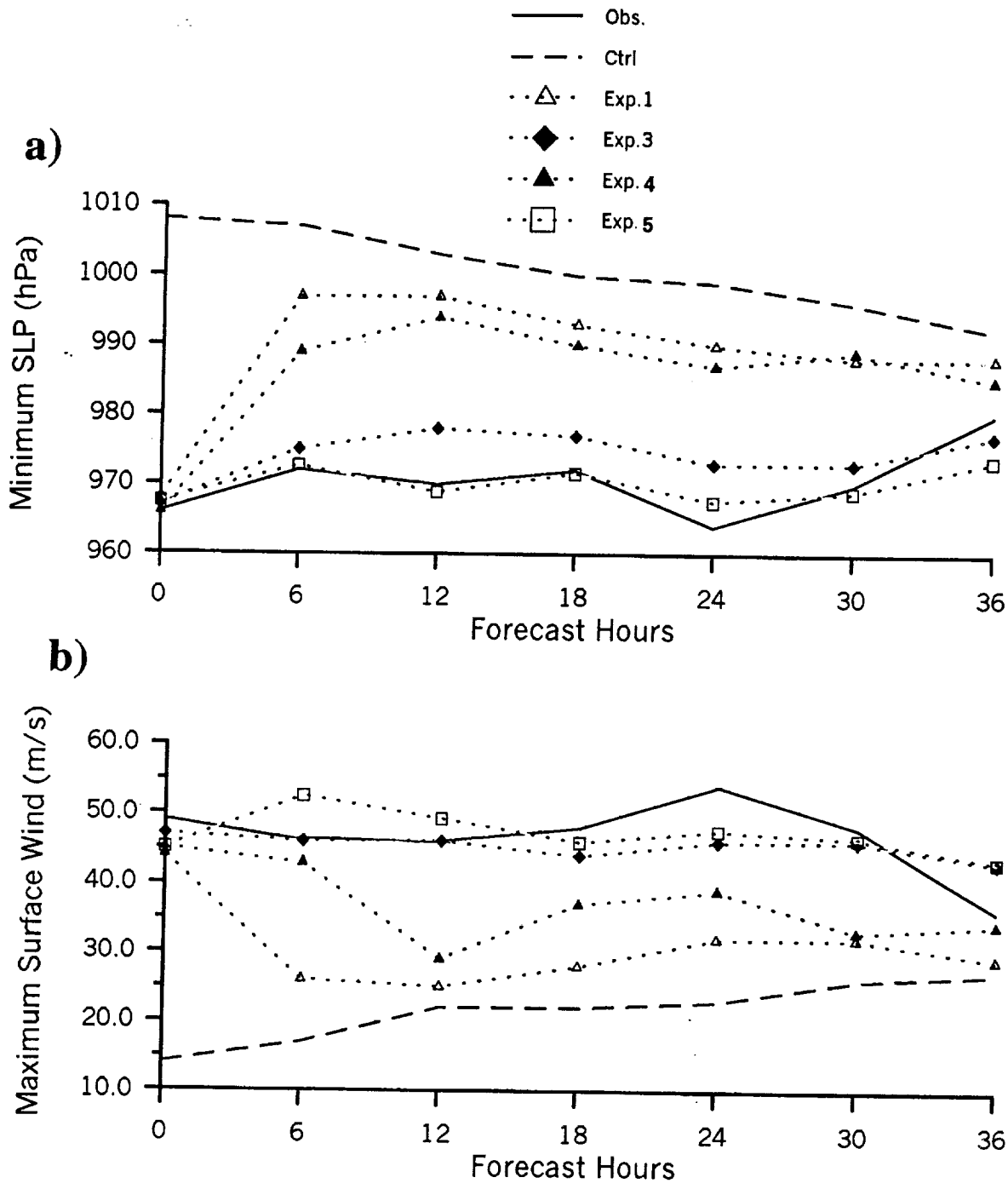
a)
Obs.
Ctrl
Exp.1
Exp.3
Exp.4
Exp.5
Minimum SLP (hPa)
1010
1000
990
980
970
960
0
6
12
18
24
30
36
Forecast Hours
b)
Maximum Surface Wind (m/s)
60.0
50.0
40.0
30.0
20.0
10.0
0
6
12
18
24
30
36
Forecast Hours

Fig. 13

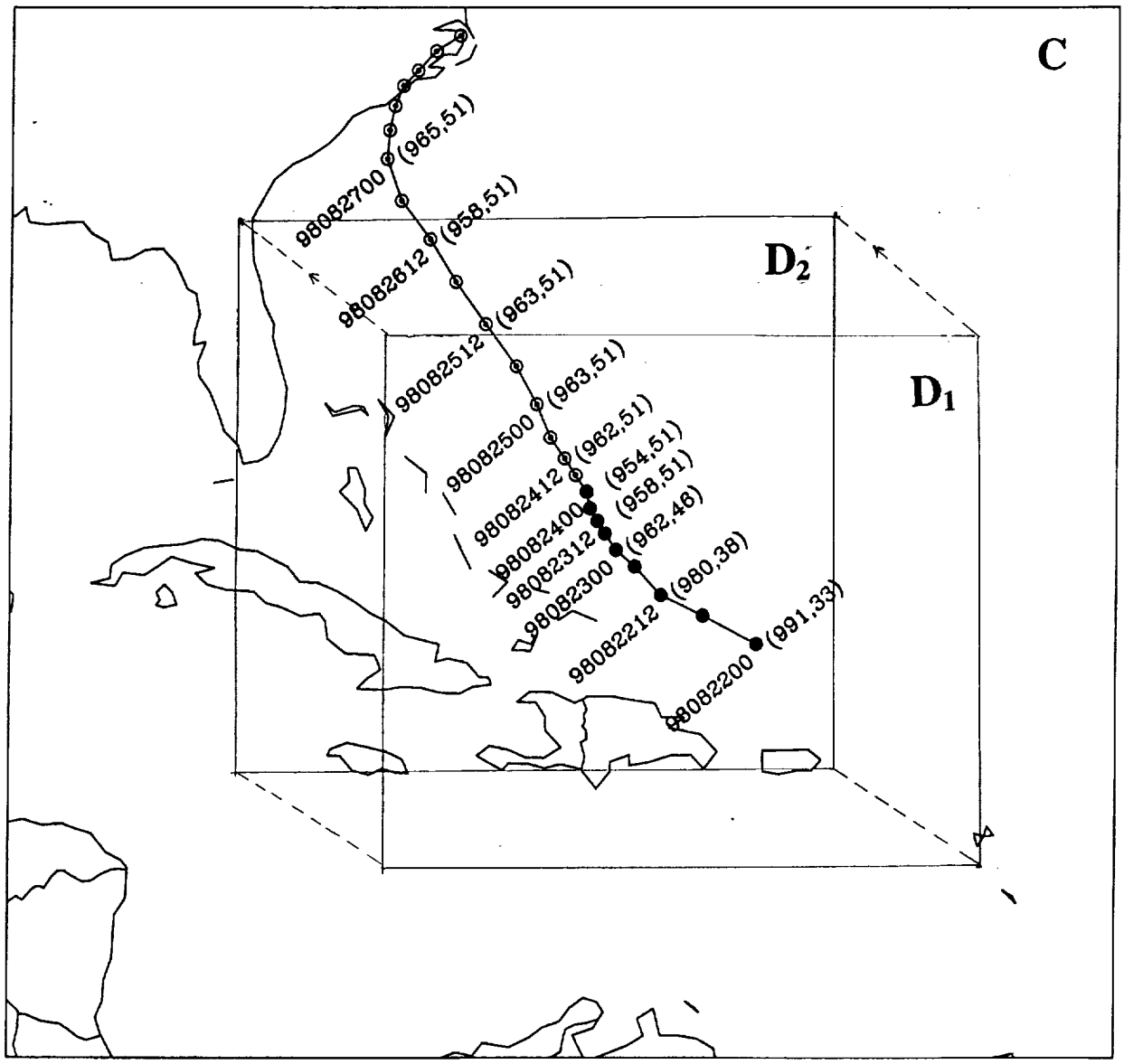
C
D2
D1
98082700
(965,51)
98082612
(958,51)
(963,51)
98082512
(963,51)
98082500
(962,51)
98082412
(954,51)
(958,51)
98082400
98082312
(962,46)
98082300
(980,38)
98082212
(991,33)
98082200

Fig. 14

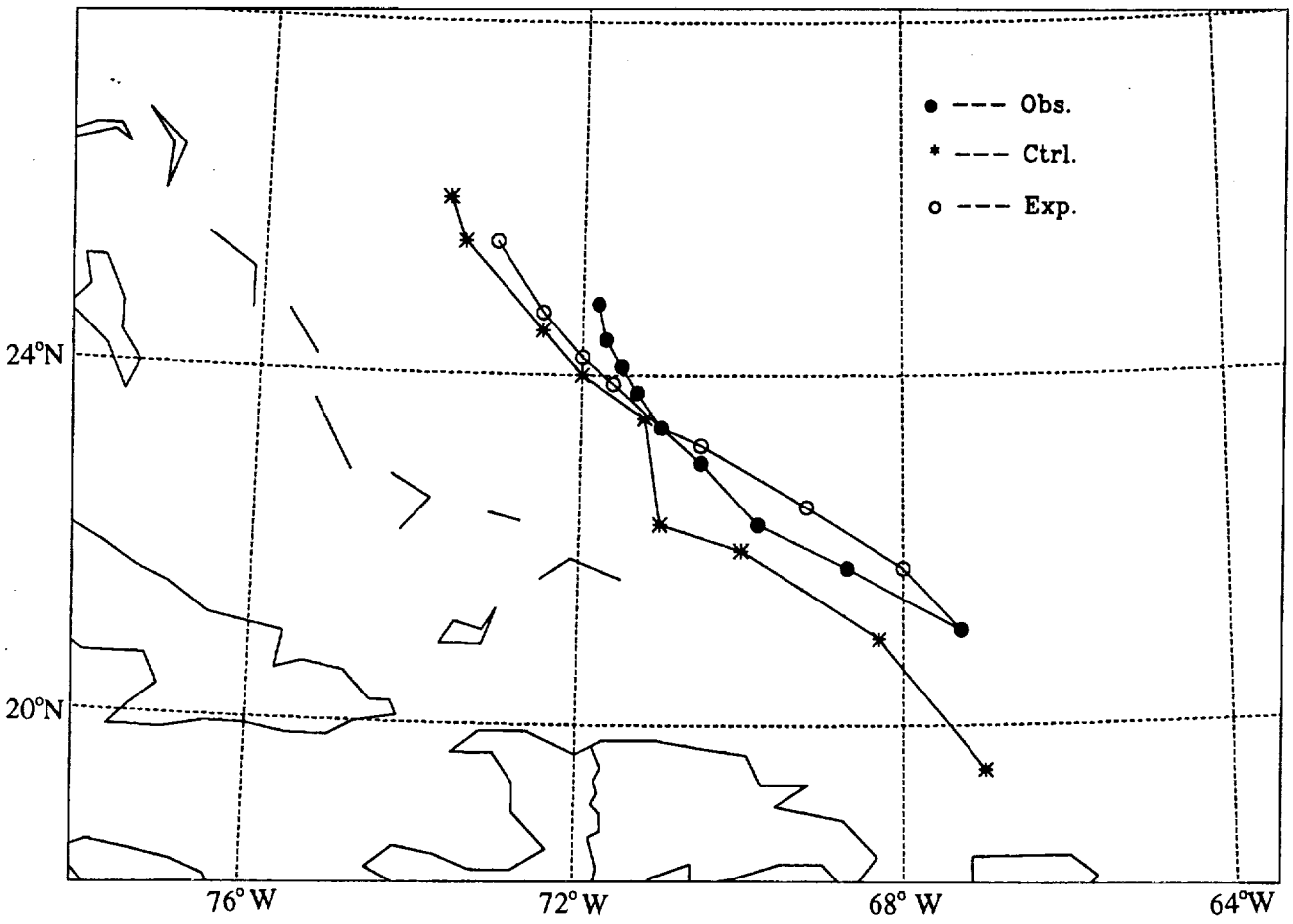

Fig. 15

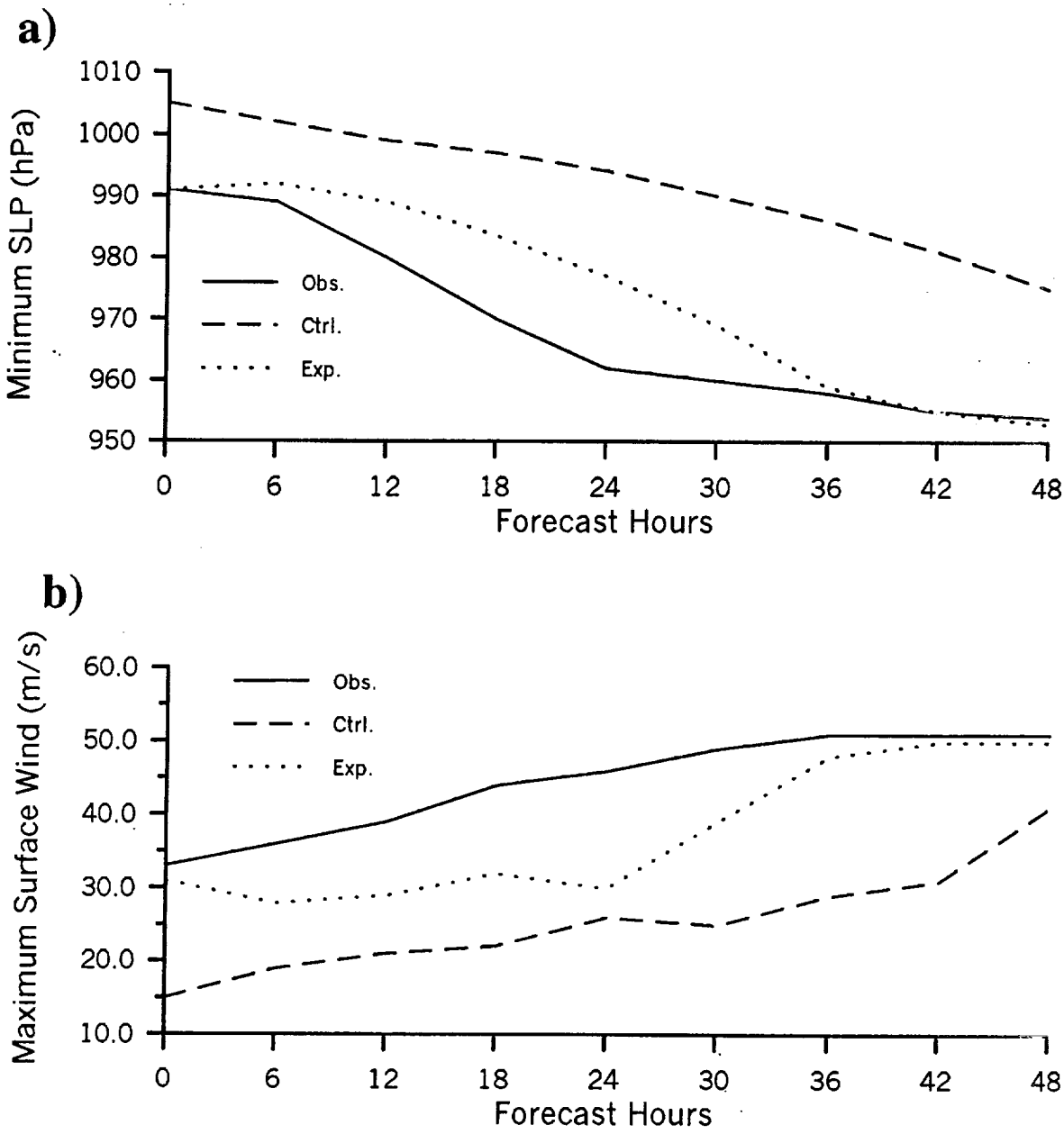
a)
Minimum SLP (hPa)
1010
1000
990
980
970
960
950
Obs.
Ctrl.
Exp.
0
6
12
18
24
30
36
42
48
Forecast Hours
b)
Maximum Surface Wind (m/s)
60.0
50.0
40.0
30.0
20.0
10.0
Obs.
Ctrl.
Exp.
0
6
12
18
24
30
36
42
48
Forecast Hours

Fig. 1b

a)

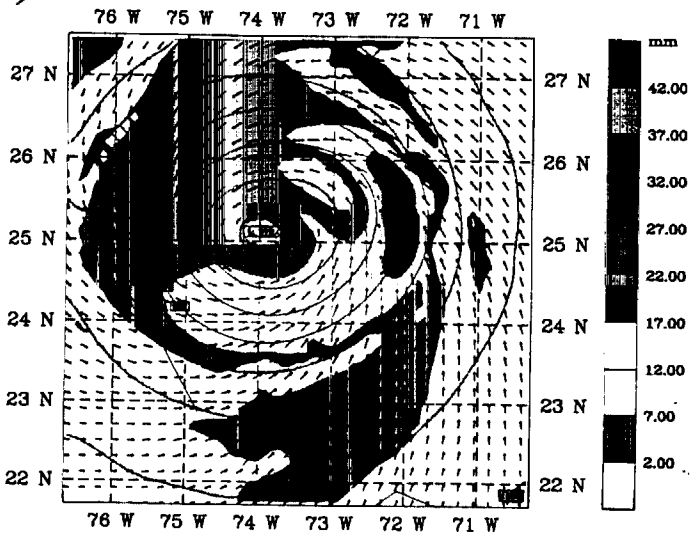

MAXIMUM VECTOR: 37.7 m s^{-1}

b)

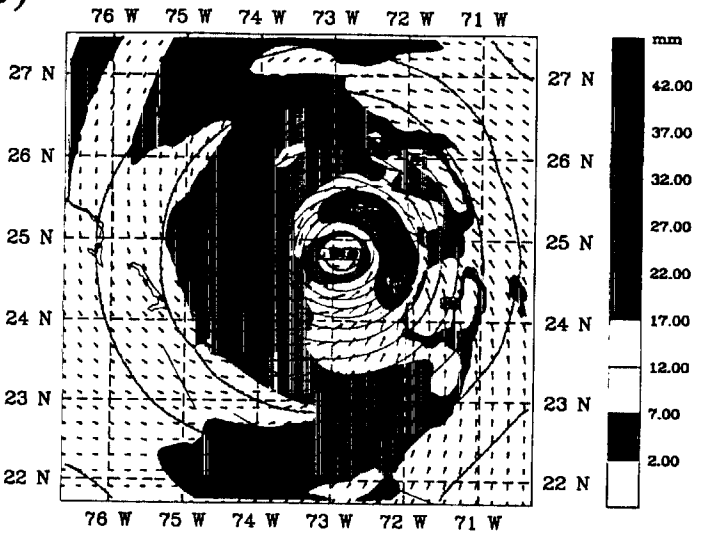

MAXIMUM VECTOR: 50.6 m s^{-1}

c)

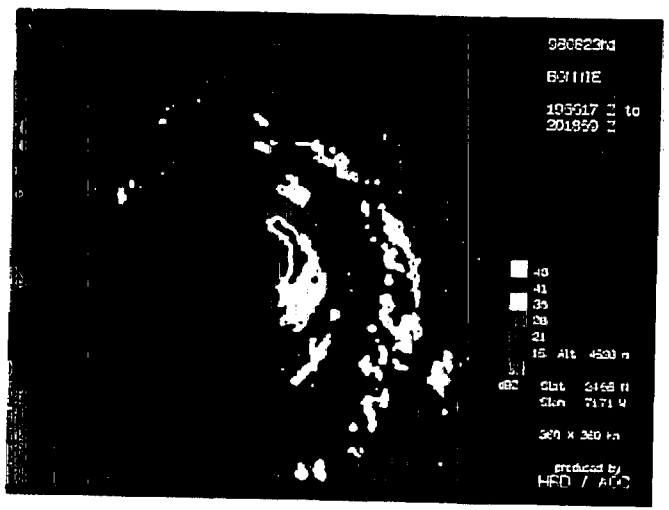

Fig. 17